

A Kinematic and Geometric Analysis of Trochoidal Waves

Andrew D Irving

Independent Researcher

Email: a_irving@btinternet.com

Ebrahim L Patel

University of Greenwich

Email: e.patel@greenwich.ac.uk

Abstract

To study the geometry of Gerstner's water wave model, we analyse the velocity of his fluid particles in a reference frame that moves with the wave. Gerstner wave profiles are cycloidal, curtate (flattened) trochoids, or prolate (extended) trochoids. We derive both the height of each profile's characterising point (cusp, inflection, or self-intersection), as well as a condition under which the arc lengths of prolate and curtate profiles coincide over a single wave cycle. We conclude with a discussion of how Galilean transformations affect particle acceleration and the geometry of their trajectories.

1 Introduction

Among the computer graphics community, extensions to a celebrated mathematical model have found favour in the rendering of rough seas (e.g. see Figure 1). Czech polymath František Gerstner pioneered the original model more than two centuries ago [1]. The model would be rediscovered independently some sixty years later in the study of rolling ships [2]. Like Gerstner, English Naval Architect William Froude and Scottish Engineer William Rankine ambitiously follow a Lagrangian approach: specifying the evolution of each fluid particle. Yet the model is surprisingly simple and produces visually realistic surface waves [3, 4].

A wind blowing across the ocean surface causes most such waves: the moving air displaces the water from a level surface equilibrium. Surface tension and gravity may then combine as restorative forces. Thus, the fluid moves back and forth. When this occurs periodically, the movement gives rise to waves. The effect of surface tension can be assumed neg-

ligible if the wavelength exceeds two centimetres. Therefore, it is gravity which dominates the fluid dynamics to give these longer waves the name of gravity waves [5].

Newton's law of inertia predicts a moving body to follow a linear path, unless that body is acted upon by some force(s) [6]. Such forces are understood to act upon the water molecules that form gravity waves. Hence, Gerstner modelled fluid particles to deviate from linear trajectories, following curved orbits instead. As a result of this deviation, the wave profiles that Gerstner's fluid particles generate are not sinusoidal, but trochoidal.

In the rest of this paper, we highlight the role of particle velocity in the differential geometry of Gerstner waves: their curvature, changes in concavity, singularities, and arc length.

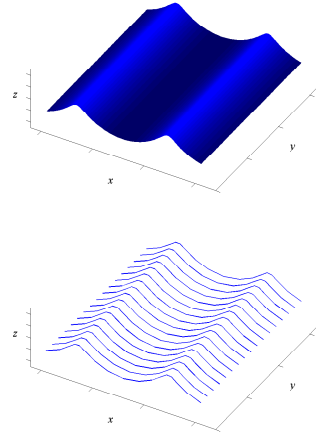


Figure 1: Simulation of [7]. Surface governed by (1) and $y = y$ at time t (top). Cross sections defined by displaying surface only for integer values of y (bottom). Gerstner's model (see (1)) describes the $y = 0$ cross section.

2 Fluid particles: Cross section of gravity waves

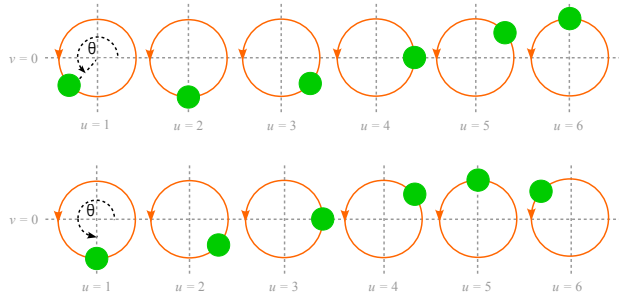


Figure 2: Sample of surface particles (green) at time t (top) and an eighth of a cycle later (bottom). In the xz -plane, a particle subtends an angle θ at the centre of a fixed orbit (orange). Here, we employ (1) using $\omega > 0$, $r < 1/2$, and only integer values of u .

Let us begin by introducing Gerstner's model. A snapshot of an ocean wave may show it to be a regular pattern of peaks and troughs [8]. None of these peaks or troughs are single points. Instead, Gerstner treats each peak or trough as a straight line. All such lines are parallel (e.g. see Figure 1). In formal language, Gerstner assumes the ocean surface to be a *two-dimensional wave*.

Figure 1 illustrates the great advantage of such a model. Any cross section of the wave which is perpendicular to a linear peak or trough is equivalent. We can therefore study the behaviour of a two-dimensional wave through any such cross section.

Gerstner pictures the two-dimensional wave in xyz -space such that one of his equivalent cross sections lies entirely in the xz -plane (as in Figure 1). For any u and $v \leq 0$, Gerstner proposes there to be a fluid particle of coordinates,

$$x = r \cos \theta + u \quad , \quad z = r \sin \theta + v \quad (1)$$

within that cross section.

The particle subtends an angle of θ at a fixed centre. That centre has coordinates (u, v) in the xz -plane (e.g. see Figure 2). Angle $\theta = \omega t + Gu$ increases by ω radians with every unit of time t that passes (making ω the particle's angular frequency and Gu the initial θ , where ω and G are non-zero parameters).

Hence, this particle traces a counterclockwise circular orbit around (u, v) over time when $\omega > 0$. Depending on the altitude of its centre, this orbit has radius $r = e^{mv}/m$, where $m > 0$ is a constant [2].

3 Composition

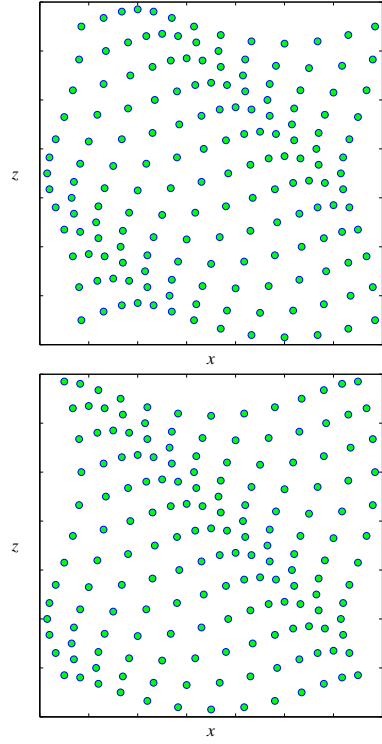


Figure 3: Our simulation of Emma Phillips' animation in [9]. One hundred and sixty nine green dots at time t (top) and later instant (bottom). Collectively, dots generate waves which travel in directions of decreasing x and decreasing z .

Even outside the computer graphics community, Gerstner's fluid particles have made an impression, thanks to an animation that has been widely imitated online (e.g. see Figure 3). Here, we first prove Phillips' animation to be an adaptation of Gerstner's work. As such, the animation is instructive as a first introduction to the structure of water waves.

In [9], Phillips' dots perform uniform circular motion such that all dots share a single fixed speed. Perhaps unexpectedly then, neighbouring dots draw closer over one time period before pulling apart over

the next (see Figure 3). As we shall prove, this is no optical illusion.

Behind Emma Phillips' eye-catching compositions are 169 dots tracing circular paths of radius $1/m$. Given an integer $u \in [-6, 6]$ and an integer $v \in [-6, 6]$, Phillips renders a dot which subtends an angle of $\omega t + Gu + Gv$ at (u, v) in the xz -plane [10]. Hence, Gertner's model governs those dots defined by Phillips' u values and $v = 0$.

Such a sample is enough to show us how a Gerstner wave propagates. As Figures 2 and 4 illustrate, the peaks and troughs of this wave are just points of constant θ which advance from one dot to another [11]. In Figure 2 for instance, the peak is a point where $\theta = 5\pi/2$ while the trough is a point where $\theta = 3\pi/2$.

Let P be the point on Phillips' Gerstner wave where θ is a constant, c . Let D be the dot which orbits $(b, 0)$ in the xz -plane. Thus, P coincides with D if and only if D subtends an angle of c at $(b, 0)$. This occurs when D has coordinates,

$$x = r \cos c + b \quad (2)$$

$$z = r \sin c \quad (3)$$

noting we have simply input $\theta = c$ and $(u, v) = (b, 0)$ into (1). This locates P for any given b .

However, we wish to be able to locate P more generally. Using $\theta = c$, we can replace b in (2) with $(c - \omega t)/G$. The resulting (2) and (3) gives us,

$$Gz + Gx = Gr \cos c + Gr \sin c + c - \omega t \quad (4)$$

which locates P at time t . Therefore, the time-derivative of (4),

$$\frac{dz}{dt} + \frac{dx}{dt} = -\frac{\omega}{G} \quad (5)$$

governs the velocity of P . Unlike (4), (5) does not depend on c . This independence of c tells us that (5) governs not just P , but any peak or trough in Figures 2 or 4.

Those peaks or troughs maintain fixed heights. As such, they are governed by $dz/dt = 0$. By substituting $dz/dt = 0$ into (5), we find their velocity \mathbf{P} to be $dx/dt = -\omega/G$. According to (1) then, D exhibits motion in both the transverse and longitudinal directions to a passing wave. To this extent, D emulates a water molecule [12].

Further reinforcing this comparison, the derivatives of (1) show the velocity of D to be,

$$\mathbf{D} = -r\omega(\sin \theta) \mathbf{i} + r\omega(\cos \theta) \mathbf{k} = -\omega z \mathbf{i} + \omega(x - b) \mathbf{k} \quad (6)$$

at time t , where \mathbf{i} and \mathbf{k} are unit vectors in the horizontal direction and the vertical direction respectively. Dot D thus behaves like a water molecule: moving with an oncoming wave at its peaks (where $x = b$ and $z = r$ in (6)) and against the wave at its troughs (where $x = b$ and $z = -r$ in (6)) [13].

Although fluid moves forward with a water wave at its peaks, Stokes predicted in 1880 that the wave would become unstable if fluid were to move forward faster than the wave itself [14]. Or if you prefer, the wave will *break* if fluid moves forward relative to the wave.

Fluid particles are thus typically modelled to flow backwards relative to the forward-moving surface wave [15] (as in Figure 4). With respect to the wave that moves forward with velocity \mathbf{P} , D does not trace a circular path with velocity \mathbf{D} . Instead, the laws of Galilean relativity dictate that D must move with a velocity,

$$\mathbf{D} - \mathbf{P} = \omega \left(\frac{1}{G} - r \sin \theta \right) \mathbf{i} + \omega(r \cos \theta) \mathbf{k} \quad (7)$$

that we shall denote \mathbf{R} [16, 17]. Hence, fluid particles flow backwards relative to their wave when the horizontal component of \mathbf{R} has the opposite sign to that of \mathbf{P} . Consequently, water waves remain stable when $rG < 1$.

Remark. The horizontal components of \mathbf{R} and \mathbf{P} have opposite signs if $(1/G) - r \sin \theta > 0$. Given the left hand side of this inequality has minimal value $(1/G) - r$, the inequality holds for all θ when $rG < 1$.

Equation (7) tells us how water behaves in the eyes of sailors who match the wave velocity. According to (7), such sailors will perceive fluid particles to trace an (upside-down) *trochoid* [18]. This trochoidal shape can be seen in Nature, on the surface of ocean waves [5]. This is no coincidence. As Figure 4 illustrates, sailors perceive fluid moving along the surface of the ocean wave.

By studying particles from this perspective, we learn about the waves they trace. When $r < 1/G$

in (7), the horizontal component of \mathbf{R} strictly increases in size from peak to trough. Fluid particles therefore travel further backward in tracing the lower half of a stable trochoidal wave cycle than they do in tracing its upper half. Relative velocity \mathbf{R} thus predicts the lower half of any stable trochoidal wave cycle to be wider than its upper half [19]. Whether the wave is stable or unstable,

$$|\mathbf{R}| = |\omega| \sqrt{\frac{1}{G^2} - \frac{2}{G} r \sin \theta + r^2} \quad (8)$$

defines the speed that D exhibits in tracing the trochoidal wave profile. With respect to any such cycle, (8) shows that the speed of the fluid particles is negatively correlated to their height.

As two such particles rise towards a trochoidal peak, (8) tells us that the leading (higher) particles is the slower at each instant. Over this period, the trochoidal arc length between the two therefore decreases. As two such particles fall towards a trough, (8) tells us that the leading (now lower) particle is the faster at each instant. Over this period, the trochoidal arc length between the two therefore increases.

The composition of [9] reflects this. When dot D subtends an angle of $\theta \equiv \frac{\pi}{2} \bmod 2\pi$ at $(x, z) = (b, 0)$, D is closer to dots which orbit $(x, z) = (b \pm 1, 0)$ than it is when D subtends an angle of $\theta \equiv \frac{3\pi}{2} \bmod 2\pi$ at $(x, z) = (b, 0)$ (see Figure 2).

4 Curvature

In the previous section, we began to see how \mathbf{R} - the velocity of water in a sailor's frame of reference - can communicate the structure of water waves. To explore this structure more deeply, we shall introduce the mathematics that most readily decipher acceleration.

As Figure 5 highlights, Phillips' fluid particle D traces the trochoidal profile of a Gerstner wave with acceleration $d\mathbf{R}/dt$. Using (7),

$$\frac{d\mathbf{R}}{dt} = \frac{d\mathbf{D}}{dt} - \frac{d\mathbf{P}}{dt} = -r\omega^2(\cos \theta) \mathbf{i} - r\omega^2(\sin \theta) \mathbf{k}. \quad (9)$$

Given $d\mathbf{P}/dt = 0$, equation (9) says what at first seems counterintuitive: $d\mathbf{R}/dt = d\mathbf{D}/dt$. Hence, a body that alternately quickens and slows along a

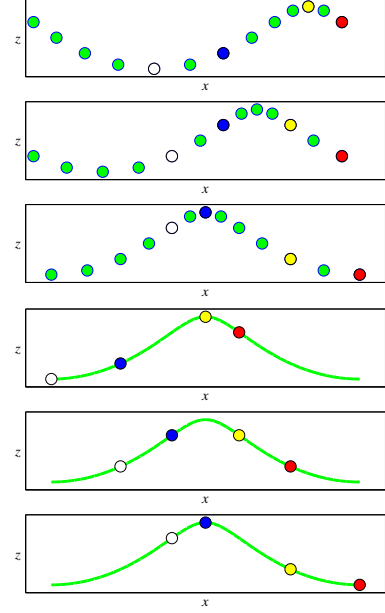


Figure 4: Sample of Phillips' dots at three moments spanning a third of a period (t increases top to bottom). In a fixed frame (upper images), dots trace circular paths with velocity \mathbf{D} and wave moves leftward. In a wave cycle's frame (lower images), the same dots have velocity \mathbf{R} , moving rightward as they trace a (green) trochoidal cycle ($rG < 1$ here).

trochoidal path (see (8)) changes velocity at the same rate as a body which travels at constant speed along a circular path (see (6)).

This is no paradox. When a body traces a curved path with variable speed $|\mathbf{v}|$, the direction of motion changes at one rate while the speed changes at another rate. As in equation (9), a horizontal component can be apportioned fractions of both rates. So too a vertical component. Acceleration can thus prove difficult to interpret. Hence, a preferred decomposition of acceleration is,

$$\frac{d\mathbf{v}}{dt} = \frac{d}{dt} \left(|\mathbf{v}| \frac{\mathbf{v}}{|\mathbf{v}|} \right) = \frac{d}{dt} (|\mathbf{v}| \mathbf{T}) = \frac{d|\mathbf{v}|}{dt} \mathbf{T} + |\mathbf{v}| \frac{d\mathbf{T}}{dt}. \quad (10)$$

Equation (10) separates the two rates at the heart of acceleration: $d|\mathbf{v}|/dt$ and $d\mathbf{T}/dt$. While the former equals the rate of change in *speed*, the significance of the latter is perhaps less obvious. In fact, $d\mathbf{T}/dt$ is the rate of change in the *direction of motion*. Let us explain.

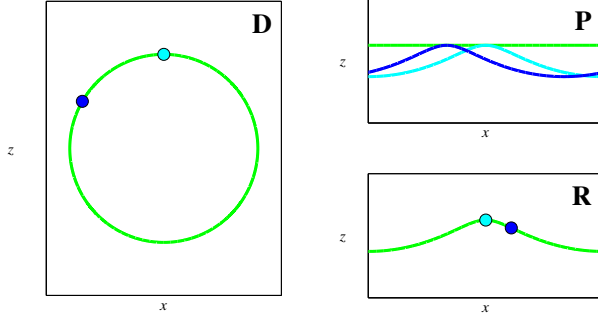


Figure 5: Trajectory and associated velocity of fluid particle illustrated: in fixed frame (left), and in frame of the wave (bottom right) ($\mathbf{R} = \mathbf{D} - \mathbf{P}$, where \mathbf{P} defines the (phase) velocity of the wave). Paths traced by particles and wave peak marked in green. Positions of particles and peaks marked at time t (cyan) and a fraction of a cycle later (blue).

As a unit vector, $\mathbf{T} = \mathbf{v}/|\mathbf{v}|$ cannot stretch or shrink over time: turning is all that \mathbf{T} can do. Therefore, $d\mathbf{T}/dt$ - the rate of change in \mathbf{T} over time - is simply the rate at which \mathbf{T} turns. Given $|\mathbf{v}|$ is just a scalar, the direction of $\mathbf{T} = \mathbf{v}/|\mathbf{v}|$ must equal the direction of \mathbf{v} . Hence, \mathbf{v} and \mathbf{T} turn at the same rate. Consequently, $d\mathbf{T}/dt$ is the rate of change in the direction of velocity \mathbf{v} .

By separating this rate from the rate at which vector \mathbf{v} stretches, equation (10) can distinguish $d\mathbf{D}/dt$ and $d\mathbf{R}/dt$. As Figure 6 illustrates, stretching rate $d|\mathbf{v}|/dt = 0$ when $\mathbf{v} = \mathbf{D}$: the velocity vector turns without stretching as a body performs uniform circular motion. In contrast, $d|\mathbf{v}|/dt \neq 0$ when $\mathbf{v} = \mathbf{R}$: the velocity vector elongates and shortens as a body traces a trochoidal profile.

At first, (10) seems otherwise daunting to compute. Fortunately, we can extract value without computing each term. We exploit a simple fact: \mathbf{T} is parallel to itself. It follows that, $\mathbf{T} \cdot \mathbf{T} = |\mathbf{T}||\mathbf{T}|$. Given \mathbf{T} is a unit vector, this means $\mathbf{T} \cdot \mathbf{T} = 1$. By differentiating both sides, we find that,

$$\mathbf{T} \cdot \frac{d\mathbf{T}}{dt} + \frac{d\mathbf{T}}{dt} \cdot \mathbf{T} = \frac{d}{dt} (1) \implies 2 \left(\mathbf{T} \cdot \frac{d\mathbf{T}}{dt} \right) = 0 \quad (11)$$

i.e. the dot product of \mathbf{T} and $d\mathbf{T}/dt$ is zero: they are *perpendicular* vectors.

This is the final property we needed to take full

advantage of (10). As $\mathbf{T} = \mathbf{v}/|\mathbf{v}|$ told us, \mathbf{T} points in the direction of motion. Hence, \mathbf{T} is *tangent* to a path traced by a body of velocity \mathbf{v} . As (11) just told us, $d\mathbf{T}/dt$ is orthogonal to \mathbf{T} . Thus $d\mathbf{T}/dt$ is *normal* to that same path. Equation (10) resolves $d\mathbf{v}/dt$ into $a_T \mathbf{T}$ and $a_N d\mathbf{T}/dt$: components we now know to be orthogonal to one another.

It follows that the acceleration $d\mathbf{v}/dt$ is the hypotenuse of a right-angled triangle with legs $a_T \mathbf{T}$ and $a_N d\mathbf{T}/dt$. By the Pythagorean theorem then,

$$\left| \frac{d\mathbf{v}}{dt} \right|^2 = |a_T \mathbf{T}|^2 + \left| a_N \frac{d\mathbf{T}}{dt} \right|^2$$

which means that,

$$\left| \frac{d\mathbf{T}}{dt} \right|^2 = \left(\frac{1}{|\mathbf{v}|} \right)^2 \left(\left| \frac{d\mathbf{v}}{dt} \right|^2 - \left(\frac{d|\mathbf{v}|}{dt} \right)^2 \right) \quad (12)$$

proving we do not need to differentiate \mathbf{T} to obtain $|d\mathbf{T}/dt|$.

Now that we know \mathbf{T} is unit tangent to the path traced by a body of velocity \mathbf{v} , it is clear that the derivative of \mathbf{T} can be interpreted geometrically. Namely, $d\mathbf{T}/dt$ is the rate at which the tangent turns as that body traces its path. We can thus infer that $|d\mathbf{T}/dt|$ must be related to that path's *curvature*: how rapidly \mathbf{T} turns per unit length of path. Indeed, curvature $\kappa = |d\mathbf{T}/dt|/|\mathbf{v}|$ by definition [8].

Combining this formula with (12) reveals how we can derive a geometric attribute of a body's path (curvature κ) entirely from a physical attribute of that body (velocity \mathbf{v}). In this way, (12) confirms that a body with velocity \mathbf{D} traces a (circular) path of constant curvature $1/r$. By contrast, a body of velocity \mathbf{R} traces a (trochoidal) path of variable curvature defined by,

$$\kappa^2 = \frac{\omega^4}{|\mathbf{R}|^4} \left(r^2 - \frac{r^2 \omega^2 \cos^2 \theta}{G^2 |\mathbf{R}|^2} \right) \quad (13)$$

wherever $|\mathbf{R}| \neq 0$. Recall that $\cos \theta = 0$ at both the highest and lowest points in that path. Hence, (13) says that $\kappa = r\omega^2/|\mathbf{R}|^2$ at such points when $|\mathbf{R}| \neq 0$. Given $|\mathbf{R}|$ is negatively correlated to the altitude (see (8)), κ proves trochoidal waves are sharper at their peaks than at their troughs when $|\mathbf{R}| \neq 0$: a feature mirrored by ocean waves.

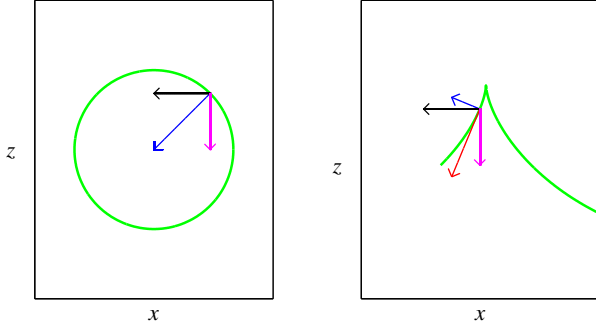


Figure 6: Components of acceleration highlighted for paths (green) traced by particles of velocity \mathbf{D} (left) and \mathbf{R} (right). At points defined by $\theta = 2\pi/8$, the horizontal components (black) are equal and vertical components (pink) are equal. However, tangential components (red) are not equal and normal components (blue) are not equal.

5 Concavity

In the previous section, we saw how changes to \mathbf{R} - the velocity of a particle tracing Gerstner's trochoidal wave profile - generates that profile's curvature. Here, we interrogate that curvature to expose the three distinctive types of trochoidal wave.

Primitive animations might depict the ocean surface as a sine wave. A sinusoid bends as sharply at peaks as it does at troughs. Let us contrast this with a trochoidal counterpart: the curvature is $r/(1/G) - r|^2$ at peaks and $r/(1/G) + r|^2$ at troughs (see (8) and (13)). Visually then, a trochoidal wave and a sine wave actually become harder to distinguish as r becomes a smaller fraction of $1/G$.

This is revealing. If a trochoidal wave may or may not look like a sine wave, it follows that two Gerstner waves may differ greatly in shape. Equation (13) suggests where we might look for fundamental differences between Gerstner waves. Consider for instance whether or not the values of r and G dictate that $|\mathbf{R}| = 0$.

Without wishing to pre-empt ourselves, these zeros mark points of distinguishing geometry. Let us explain why. A body has speed $|\mathbf{v}| = 0$ if and only if that same body has velocity $\mathbf{v} = \mathbf{0}$. Where both $\mathbf{v} = \mathbf{0}$ and $|\mathbf{v}| = 0$, we can define no unit tangent $\mathbf{T} = \mathbf{v}/|\mathbf{v}|$ to a body's path. Where \mathbf{T} does not exist,

no derivative of \mathbf{T} exists. In short, bodies of velocity $\mathbf{v} = \mathbf{0}$ lie at points where $\kappa = |\mathbf{dT}/dt|/|\mathbf{v}|$ is an indeterminate form. Using (7), it is clear that such points are found on trochoidal waves where,

$$\mathbf{R} = \mathbf{0} \iff (\cos \theta, \sin \theta) = \left(0, \frac{1}{rG}\right). \quad (14)$$

Figure 2 illustrates that $\cos \theta = 0$ at peaks (where $\sin \theta = 1$) and troughs (where $\sin \theta = -1$) only. Given $G > 0$, $\sin \theta = -1$ is incompatible with (14). Therefore, equation (14) predicts the velocity of a our fluid particle vanishes if and only if $\sin \theta = 1 = 1/rG$. Or if you prefer, our particle's velocity vanishes exclusively at the peaks of $rG = 1$ trochoids.

When $rG = 1$, it is telling that fluid particles should trace trochoidal paths with velocity,

$$\mathbf{R} = r\omega (1 - \sin \theta) \mathbf{i} + r\omega (\cos \theta) \mathbf{k} \quad (15)$$

according to (7). Thus, Gerstner's particles bear the character of particles tracing an (upside-down) cycloid [18].

Equation (15) not only identifies this form of trochoid as a cycloid, but can also be used to classify the $rG = 1$ peaks geometrically. Velocity \mathbf{R} does this by giving us the cycloidal slope S as a ratio of its components. Although we cannot determine $S = \cos \theta/(1 - \sin \theta)$ at cycloidal peaks (where $\theta = a = 2\pi q + \pi/2$ for $q \in \mathbb{Z}$), we can evaluate the limit of S as θ approaches a . While this is not possible by directly substituting $\theta = a$ into S , we can apply L'Hôpital's rule to find that,

$$\lim_{\theta \rightarrow a} S = \lim_{\theta \rightarrow a} \frac{\frac{d}{d\theta}(\cos \theta)}{\frac{d}{d\theta}(1 - \sin \theta)} = \lim_{\theta \rightarrow a} \tan \theta$$

which means that,

$$\lim_{\theta \rightarrow a} S = \begin{cases} +\infty, & \text{as } \theta \rightarrow a^- \\ -\infty, & \text{as } \theta \rightarrow a^+ \end{cases} \quad (16)$$

As (16) says, the slope of a cycloidal wave is positive on one side of any peak, but negative on the other [20]. When tracing a cycloid then, a fluid particle makes sharp about-turns at peaks, proving such peaks to be *vertical cusps* [21]. The rapid change in direction corresponds to an infinitely fast rotation of the tangent, which is precisely what infinite curvature measures.

Let us now shift our focus to points of zero curvature. Given the curvature of a trochoidal wave is $\kappa = |\mathbf{dT}/dt|/|\mathbf{R}|$ by definition, it is clear that $\kappa = 0$ if and only if both $|\mathbf{dT}/dt| = 0$ and $|\mathbf{R}| \neq 0$. Geometrically then, points of zero curvature are those where tangent $\mathbf{T} = \mathbf{R}/|\mathbf{R}|$ exists (since $|\mathbf{R}| \neq 0$), but has stopped turning (since $|\mathbf{dT}/dt| = 0$).

Using the right hand side of (12), points on our wave have zero curvature if and only if they satisfy,

$$r^2 = \frac{r^2 \omega^2 \cos^2 \theta}{G^2 |\mathbf{R}|^2} \implies (rG - \sin \theta)^2 = 0 \quad (17)$$

without violating our $|\mathbf{R}| \neq 0$ condition.

No $rG > 1$ satisfies (17), as $\sin \theta \leq 1$. Nor can $rG = 1$ satisfy (17), as (14) confirms that $\sin \theta = rG = 1$ violates our $|\mathbf{R}| \neq 0$ condition on (17). Simply put, trochoidal profiles possess points of zero curvature if and only if $rG < 1$.

Equations (14) and (17) reveal the altitude of points of notable curvature. As Figure 2 illustrates, the value of $r \sin \theta$ defines the altitude of our fluid particle, D . Hence, equation (14) proves that cycloidal points of infinite curvature have altitude $z = 1/G$ while (17) proves points of zero curvature have altitude $z = r^2 G$.

To classify points of zero curvature geometrically, we use (7) to inspect the trochoidal slope S_T . More specifically, we inspect,

$$dS_T/dt = \frac{r^2 \omega - \frac{r\omega}{G} \sin \theta}{\left(\frac{1}{G} - r \sin \theta\right)^2} = \frac{\omega \left(r^2 - \frac{1}{G} z\right)}{\left(\frac{1}{G} - z\right)^2} \quad (18)$$

to determine how tangent \mathbf{T} behaves as a fluid particle rises or falls through altitude $z = r^2 G$. Since points of zero curvature lie on the $rG < 1$ wave, they lie below trochoidal peaks (where $z = r$) and above the rest position (where $z = 0$).

As (18) shows then, dS_T/dt is positive at the rest position, zero at points of zero curvature, and negative at the $rG < 1$ peaks. Put simply, this tells us tangent \mathbf{T} is turning counterclockwise as a particle rises from the rest position until it reaches an altitude of $z = r^2 G$. At this altitude, the turning pauses momentarily. As a particle rises beyond an altitude of $z = r^2 G$, the turning of \mathbf{T} resumes, but now in the clockwise direction instead. Tangent \mathbf{T} changes its direction of rotation at $z = r^2 G$. Our points of zero curvature are thus *inflections*.

In conclusion, our trochoidal profiles do not exhibit points of infinite curvature unless $rG = 1$, nor do they exhibit points of zero curvature unless $rG < 1$. Hence, tangent \mathbf{T} turns continuously in a single direction as a fluid particle traces profiles where $rG > 1$ (see Figure 7). Given this rotation results in opposite horizontal tangents at peaks and troughs when $rG > 1$ (see (7)), we conclude the profile *self-intersects*.

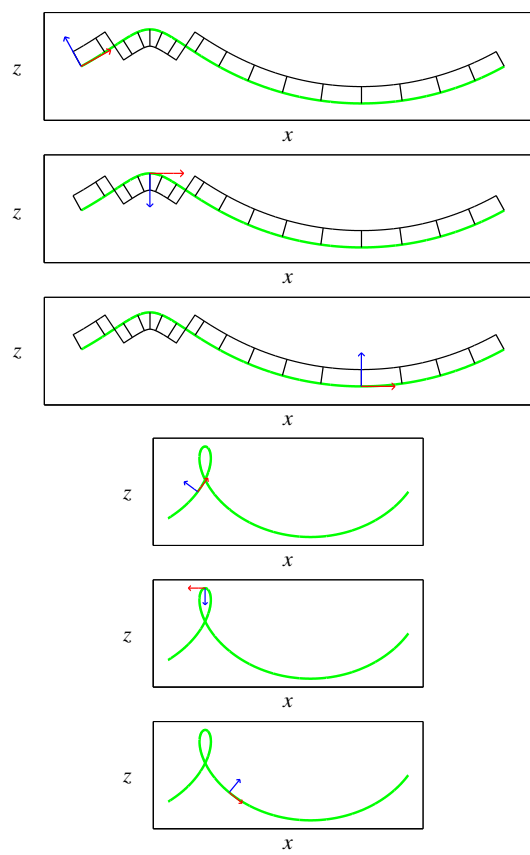


Figure 7: Tangent $\mathbf{T} = \mathbf{R}/|\mathbf{R}|$ (red) and corresponding normal $\mathbf{N} = (\mathbf{dT}/dt)/|\mathbf{dT}/dt|$ (blue) to path (green) form an intrinsic coordinate system. The associated grid (black) is illustrated on the normal's side of the path. As a particle advances along the path, tangent \mathbf{T} turns toward the side of this path that \mathbf{N} points to. In upper images ($rG < 1$), \mathbf{T} is turning counterclockwise, then clockwise, then counterclockwise again. In lower images ($rG > 1$), \mathbf{T} is turning counterclockwise in all images.

6 Crossings

In the previous section, we saw how the time-evolution of $\mathbf{T} = \mathbf{R}/|\mathbf{R}|$ - the tangent to a trochoidal wave - can forecast that wave's *concavity*. As such, Gerstner's model predicts the profile of a breaking (unstable) wave to cross itself. Such profiles are physically unrealistic [22]. Where self-intersections can be precisely located though, users can truncate a wave profile accordingly.

When $rG > 1$, our trochoidal wave profile exhibits a loop and a point of self-intersection: a *node*. When such profiles are rendered using (1), a node becomes a point in space which could be occupied by two fluid particles at once.

To avoid this interpretation, let us instead view a trochoidal profile as the path traced by just one fluid particle, D . Equation (7) defines the velocity of D as it traces the profile to be \mathbf{R} . By integrating \mathbf{R} with respect to t , we therefore recover the trochoidal profile that D traces over time:

$$\int \mathbf{R} dt = \left(r \cos \theta + \frac{\omega}{G} t + C_1 \right) \mathbf{i} + (r \sin \theta + C_2) \mathbf{k} \quad (19)$$

where C_1 and C_2 are constants of integration. By setting t equal to zero, we obtain $C_1 = x_0 - r \cos(Gb)$ and $C_2 = z_0 - r \sin(Gb)$, where x_0 and z_0 are the initial coordinates of D .

Featured in Figure 7, trochoidal wave profiles appear to exhibit a vertical line of symmetry through any chosen trochoidal peak, say p . To prove this line exists, we suppose D to be at peak p when $t = 0$. Hence, D has initial coordinates $(x_0, z_0) = (b, r)$ and an initial phase of $\theta = Gb = \pi/2 + N2\pi$ for some $N \in \mathbb{Z}$. Using $N = 0$, let us compare the positions of D at $t = f$ and $t = -f$.

Given $Gb = \pi/2$, four values follow: $\sin(Gb) = 1$, $\cos(Gb) = 0$, $C_1 = x_0$ and $C_2 = 0$. By applying sum formulae to the trigonometric functions of (19) and substituting these four values into the results, we find that D has general coordinates,

$$\chi = -r \sin(\omega t) + \frac{\omega t}{G} + b \quad , \quad z = r \cos(\omega t) \quad (20)$$

in this example. As Galilean relativity dictates, the horizontal coordinate of D above, χ , is equal to $x - \omega t/G$.

Since cosine is an even function, we can conclude that D has the same height at $t = \pm f$ when D begins at a peak. In our example, $\chi - x_0$ at $t = f$ is the negative of $\chi - x_0$ at $t = -f$ since sine is an odd function. As f is arbitrary, these properties prove that a vertical line of symmetry does pass through peak p .

Any nodes must obey this line of symmetry. Let us assume that Figure 7 is not atypical of the $rG > 1$ case: there exists a single node between $\chi = x_0 - \lambda/2$ and $\chi = x_0 + \lambda/2$ when $rG > 1$, where $\lambda = 2\pi/G$ is the trochoidal wavelength. That node could not obey our line of symmetry without lying upon it. As such, our node will share the χ value of p .

When D begins at peak p then, D will reach different points on the wave when $t = f$ and $t = -f$. Except when D reaches our node. Hence, our node is the only point on the wave where χ at $t = f$ equals χ at $t = -f$ for $f \neq 0$, meaning,

$$\frac{\omega}{G} f = r \sin(\omega f) \iff \frac{\sin(\omega f)}{\omega f} = \frac{1}{rG} \quad (21)$$

holds for no point other than our node if $f \neq 0$, according to (20).

Remark. Readers may be interested to know that $\sin(\omega f)/\omega f$ is the *cardinal sine (sinc)* function of ωf . The function is undefined for $\omega f = 0$. Consequently, we need to define the function's value at $\omega f = 0$ based on the limit as ωf approaches 0. This limit is 1. By the nature of sinc functions, it follows that $\sin(\omega f)/\omega f < 1$ for all non-zero values of ωf . Therefore, as we would expect, we cannot solve (21) for any $rG \leq 1$.

In general, solving (21) for f is not straightforward. One specific solution is self-evident though. By comparing the numerators and denominators of (21), we can see that $\sin(\omega f) = 1$ (and therefore $\cos(\omega f) = 0$) when $\omega f = rG$. Substituting these expressions into (20), we can thus establish that the node which lies on the line of symmetry through p has coordinates $(\chi, z) = (x_0, 0)$ when $\omega f = rG$.

We can generalise this approach by adapting equation (21) into the form,

$$\frac{\sin(\omega f)}{\omega f} = \frac{1}{rG} \iff \frac{\sin(\omega f)}{\omega f} = \frac{A}{ArG} \quad (22)$$

where $A \neq 0$ is a value to be determined. When we choose A to equal $\sin(\omega f)$, equation (22) tells us that $\omega f = ArG$. By substituting these expressions into (20), we find that a node which lies on the line of symmetry through p has coordinates,

$$(\chi, z) = (x_0, r \cos(ArG)) \quad (23)$$

when $\omega f = ArG$.

To be clear, (23) defines our node's location for a chosen value of ArG . By equating the denominators of (22), we thus obtain a value for ωf . By equating the numerators of (22), we obtain a value for $A \in [-1, 1]$. Then we obtain a value for $rG > 1$ by dividing our initially chosen ArG value by A .

Unlike inflections and cusps, nodes can lie below the rest positions of Gerstner waves. Equation (23) says that nodes have altitude $z < 0$ when,

$$\frac{\pi}{2} < ArG < \pi \iff \frac{\pi}{2A} < rG < \frac{\pi}{A}$$

noting ωf (which we set equal to ArG), the change in θ over f units of time, need not exceed π for our purposes.

Table 1: Examples of solutions to (22) and (23), where (x_0, z) mark our self-intersection's coordinates. One possible value for x_0 is b , a value we can determine using $Gb = \pi/2$ and rG values.

A	ωf	rG	x_0	z
$\frac{1}{2}$	$\frac{5\pi}{6}$	$\frac{5\pi}{3}$	$\frac{3r}{10}$	$-\frac{\sqrt{3}r}{2}$
1	$\frac{\pi}{2}$	$\frac{\pi}{2}$	r	0
$\frac{\sqrt{3}}{2}$	$\frac{\pi}{3}$	$\frac{2\pi}{3\sqrt{3}}$	$\frac{3\sqrt{3}r}{4}$	$\frac{r}{2}$
$\frac{\sqrt{2}}{2}$	$\frac{\pi}{4}$	$\frac{\pi}{2\sqrt{2}}$	$\sqrt{2}r$	$\frac{\sqrt{2}r}{2}$

7 Cycloids

In the previous section, we saw how the profiles of Gerstner's water waves exhibit (unrealistic) loops once they become overly steep. Under Gerstner's model, unstable waves manifest as *prolate* (extended) trochoids, while stable waves manifest as cycloids or *curtate* (flattened) trochoids.

By convention, trochoidal curves are generated mechanically. As a circular wheel undergoes *pure*

rolling (spinning as much as it moves forwards) along a horizontal plane, a point attached to the wheel traces a trochoidal curve. When the point is fixed to the wheel's rim, the resulting curve is a cycloid. When the point is closer to / farther from the wheel's centre, the result is a shorter / longer curve: a curtate / prolate trochoid. Determining just how much shorter or longer is the subject of this section.

As we shall go on to explain, some trochoidal curves are easier to measure than others. In understanding why this might be, let us briefly discuss an unconventional interpretation of trochoidal curves. Under Phillips' setup, all three forms of wave are generated by fluid particles that behave as though they were points on the rims of circular wheels of radii r . As the wheels roll along a horizontal plane, it is the mode of rolling which determines the form of wave profile the particle traces.

There are three modes of rolling. First, suppose $|\mathbf{D}|$, the (tangential) speed of the fluid particle, matches $|\mathbf{P}|$, the speed of the wave. Then the arc length travelled by a point on our wheel (relative to the axle) matches the distance travelled by the axle. Our wheel spins as much as it moves forwards: it exhibits pure rolling. It turns out that $|\mathbf{D}| = |\mathbf{P}|$ corresponds precisely to the case where $rG = 1$, i.e. pure rolling generates the cycloidal wave.

Secondly, suppose $|\mathbf{D}|$, the (tangential) speed of the fluid particle, exceeds $|\mathbf{P}|$, the speed of the wave. Then the arc length travelled by a point on our wheel (relative to the axle) exceeds the distance travelled by the axle. Our wheel spins more than it moves forwards: it is said to be *slipping*. It turns out that $|\mathbf{D}| > |\mathbf{P}|$ corresponds precisely to the case where $rG > 1$, i.e. slipping generates the prolate trochoidal wave.

Third, suppose $|\mathbf{D}|$, the (tangential) speed of the fluid particle, is less than $|\mathbf{P}|$, the speed of the wave. Then the arc length travelled by a point on our wheel (relative to the axle) is less than the distance travelled by the axle. Our wheel spins less than it moves forwards: it is said to be *skidding*. It turns out that $|\mathbf{D}| < |\mathbf{P}|$ corresponds precisely to the case where $rG < 1$, i.e. skidding generates the curtate trochoidal wave.

Whichever you prefer, both interpretations prove that the three forms of trochoidal wave profile are generated in three materially different ways. Per-

haps unsurprisingly then, no single closed-form expression defines the arc length of all three trochoidal forms.

Since the arc length of a trochoidal wavelength is equal regardless of which points we choose as endpoints, let us measure the arc length peak-to-peak. Using (20) in the standard formula yields:

$$L = \int_0^{\frac{2\pi}{\omega}} \sqrt{\left(\frac{d\chi}{dt}\right)^2 + \left(\frac{dz}{dt}\right)^2} dt = \int_0^{\frac{2\pi}{\omega}} |\mathbf{R}| dt$$

i.e. the arc length of a path is equal to the speed of a point tracing that path, integrated over time. This mirrors the classical relation: Distance = Speed \times Time. Using (8), we obtain:

$$L = \omega \int_0^{\frac{2\pi}{\omega}} \sqrt{r^2 + \frac{1}{G^2} - \frac{2r}{G} \cos(\omega t)} dt. \quad (24)$$

Suppose the value of rG , which determines the form of our trochoidal wave, is equal to h . If we substitute r/h for $1/G$ into (24), we can extract a common factor of r :

$$L = r\omega \int_0^{\frac{2\pi}{\omega}} \sqrt{1 + \frac{1}{h^2} - \frac{2}{h} \cos(\omega t)} dt.$$

Next, we can exploit a half-angle formula, $1 - \cos(2\psi) = 2 \sin^2 \psi$ to determine that,

$$L = 2r \int_{T=0}^{T=\pi} \sqrt{1 + \frac{1}{h^2} - \frac{2}{h} + \frac{4}{h} \sin^2 T} dT \quad (25)$$

where we made the substitution $T = \omega t/2$. In the cycloidal case, it is clear that we can integrate our expression directly since (25) becomes,

$$L = 4r \int_{T=0}^{T=\pi} |\sin T| dT = 4r \int_0^\pi \sin T dT = 8r \quad (26)$$

when $h = 1$. As (26) says, the length of a cycloidal wave cycle depends only its height. The length of any other trochoidal wave proves harder to compute, the integral that we must solve in (25) being *elliptic*, as we can show more clearly by expressing it in the following form:

$$L = 2r\sqrt{Q} \int_{T=0}^{T=\pi} \sqrt{1 - m \sin^2 T} dT \quad (27)$$

where $Q = 1 - (2/h) + 1/(h^2)$ and $m = -(4/h)/Q$, noting m assumes $Q \neq 0$ (equivalent to $h \neq 1$). It is the classical elliptic form of (27) which defines the arc length of all non-cycloidal trochoids.

Remark. Equation (27) is a complete elliptic integral of the second kind that we have reduced to one of Legendre's three *canonical* (normal) forms. The integral can be evaluated numerically using the Arithmetic-Geometric Mean (AGM) technique. Approximate analytical solutions have been proposed [23].

While (27) cannot be solved analytically, we can still make certain observations about our non-cycloidal waves. Consider two trochoidal waves: one prolate (where $r = r_1$ and $G = G_1$ such that $r_1 G_1 > 1$) and one curtate (where $r = r_2$ and $G = G_2$ such that $r_2 G_2 < 1$). Without needing to solve (24), it is clear that our curtate and prolate waves have equal peak-to-peak arc lengths when:

$$\frac{2r_1}{G_1} = \frac{2r_2}{G_2} \quad \text{and} \quad r_1^2 + \frac{1}{G_1^2} = r_2^2 + \frac{1}{G_2^2}$$

which we solve simultaneously to obtain the condition: $r_1/G_1 = r_2/G_2$. Despite their distinctive geometry, the peak-to-peak profiles of an extended wave and flattened wave are equally long (e.g. see Figure 8) when,

$$\frac{r_1 \lambda_1}{2\pi} = \frac{r_2 \lambda_2}{2\pi} \iff 2\pi r_1 \lambda_1 = 2\pi r_2 \lambda_2.$$

A point on the generating wheel's rim travels a distance of $2\pi r$ with respect to the axle, for every λ the axle travels horizontally. In short, the product of a generating wheel's rotation and translation is equal for both trochoids.

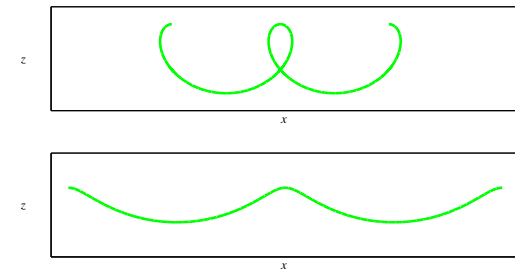


Figure 8: Two curves of equal arc length: a prolate trochoidal curve (top image: $r = 1/2$ and $G = 4$), and a curtate trochoidal curve ($r = 1/4$ and $G = 2$). A particle traces either in $4\pi/\omega$ units of time.

8 Overview: Richness and realism

Over two hundred years old, Gerstner's equations model water waves as trochoidal. Any such form is best understood by analysing \mathbf{R} , the velocity of a particle as it traverses the wave. How this velocity changes over time relates the wave structure.

By convention, velocity is considered a physical vector quantity. Nonetheless, a body's velocity \mathbf{v} can be expressed as a product of its speed $|\mathbf{v}|$ and geometrical vector \mathbf{T} : the tangent to that body's path. To judge how velocity changes over time then, we apply the product rule of differentiation to $\mathbf{v} = |\mathbf{v}|\mathbf{T}$:

$$\underbrace{\frac{d\mathbf{v}}{dt}}_{\text{Total Acceleration}} = \underbrace{\frac{d|\mathbf{v}|}{dt}\mathbf{T}}_{\text{Tangential Acceleration}} + \underbrace{|\mathbf{v}|\frac{d\mathbf{T}}{dt}}_{\text{Normal Acceleration}}. \quad (28)$$

As illustrated in Figure 7, (28) decomposes acceleration into perpendicular components: one in the direction of motion, one toward the centre of curvature [24, 25].

Each component plays a distinctive role in our analysis. Interrogating $d|\mathbf{v}|/dt$ can reveal not just how much a body of velocity \mathbf{v} is quickening or slowing but whether two bodies of velocity \mathbf{v} are drawing closer or pulling apart. This can influence the distribution of bodies traversing a single path. When $\mathbf{v} = \mathbf{R}$, fluid particles less than half a cycle apart are thus closer when one is at a peak than when one is at a trough (see Figure 4).

Interrogating the $d\mathbf{T}/dt$ of (28) tells us how much a path of tangent \mathbf{T} is turning at time t . How \mathbf{T} evolves with t thus defines the geometry of a body's path. When $\mathbf{T} = \mathbf{R}/|\mathbf{R}|$, this path is trochoidal. As (13) shows, $\mathbf{T} = \mathbf{R}/|\mathbf{R}|$ turns more rapidly at peaks than it does at trochoidal troughs, proving the peaks to be sharper.

Despite sharing these properties, any two trochoidal waves may have geometric features which distinguish them from one another. Depending on a user's choice of parameter values, rendered waves exhibit one of three features: nodes (when $rG > 1$), cusps (when $rG = 1$), or inflections (when $rG < 1$).

Let us characterise each of these features by the behaviour of tangents. Wherever two branches of a trochoidal profile cross one another, we can define two different tangents: one for each branch (as in

Figure 9). Thus, a single point on a trochoidal wave cycle - a node - exhibits multiple distinct tangents when $rG > 1$.

If users instead lower the value of rG to one, the profile becomes a cycloid: nodes degenerate into cusps, as a node's non-coincident tangents come to coincide at a cycloidal peak. Velocity \mathbf{R} vanishes at these cusps such that they exhibit no unit tangent $\mathbf{T} = \mathbf{R}/|\mathbf{R}|$ (as in Figure 9).

Visually, Gerstner waves approximate sinusoids when $rG \ll 1$. Like tangents of the latter, tangents of the former instantaneously stop turning at some height when $rG < 1$. Tangent \mathbf{T} turns clockwise above, and counterclockwise below, this height in Figures 7 and 9. Points at this height - inflections - exhibit one non-rotating tangent.

Table 2: Properties of Trochoidal waves.

	$rG < 1$	$rG = 1$	$rG > 1$
Arc length	See (27)	$8r$	See (27)
Key point p	Inflection	Cusp	Node
Altitude of p	r^2G	r	$r \cos(Arg)$
Tangents at p	1	0	2
$ dT/dt $ at p	0	N/A	Non-zero

When users choose values that dictate $rG \leq 1$, a stable wave is modelled. Otherwise, a breaking wave is represented. Whether viewed through a physical lens or through a geometric lens, let us show that Gerstner waves thus obey an intuitive stability threshold. Although not obvious at first glance, rG is equal to a fraction:

$$rG = \frac{r|\omega|}{|\omega|/G} = \frac{|\mathbf{D}|}{|\mathbf{P}|} \quad (29)$$

which exceeds one if and only if $|\mathbf{D}| > |\mathbf{P}|$. Hence, equation (29) says Gerstner's model fits with real world observation: gravity waves will break once constituent particles move faster than the waves do.

While Gerstner's profile of a breaking wave may not be realistic, we can nevertheless constructively interpret (29) geometrically. Gerstner's model predicts that a gravity wave breaks once,

$$rG > 1 \iff r \frac{2\pi}{\lambda} > 1 \iff 2r > \frac{\lambda}{\pi}. \quad (30)$$

Put simply, the right-most inequality in (30) predicts that gravity waves grow unstable once their height ($2r$) exceeds a fraction of their wavelength. Thus, Gerstner's model imitates Nature: a gravity wave will break if the surface slopes too steeply [26].

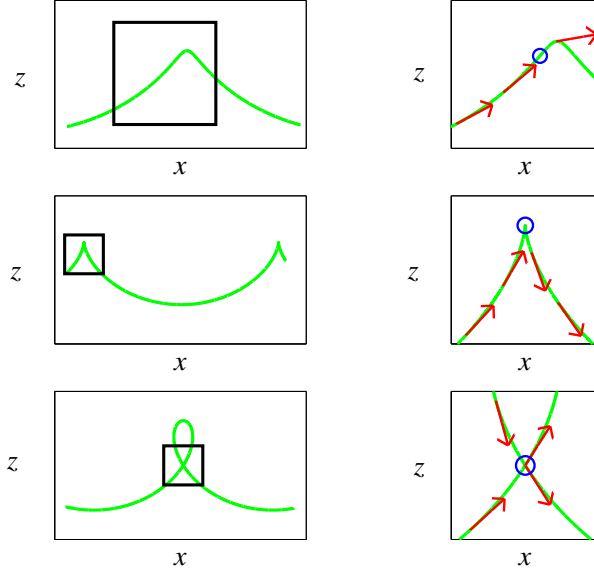


Figure 9: Gerstner waves when $rG < 1$ (top), $rG = 1$ (middle), and $rG > 1$ (bottom). Zooming out (left) and in (right) on circled points: inflection (top), cusp (middle), and node (bottom). Tangent (unit velocity) vectors (red) shown local to each point.

9 Discussion: Galilean transformations

Gerstner's fluid particles highlight a key distinction between velocity and acceleration. As \mathbf{D} and $\mathbf{R} = \mathbf{D} - \mathbf{P}$ demonstrate, the velocity of a body is relative: a change of reference frame can change the velocity. By contrast, equation (9) reveals $d\mathbf{D}/dt = d\mathbf{R}/dt$. Swapping one non-accelerating and non-rotating reference frame for another - what is called a *Galilean transformation* - cannot change the size or direction of any acceleration vector. A body's acceleration is absolute [27].

However, even acceleration vectors which are equal may decompose differently (e.g. see Figure 6). While such vectors decompose identically in a single coordinate system, differences may emerge when we

instead use the *intrinsic coordinates* of a body's motion. By applying the formula in (28) to $d\mathbf{D}/dt = d\mathbf{R}/dt$ for instance, such coordinates yield,

$$\underbrace{|\mathbf{D}| \frac{d\mathbf{T}_D}{dt}}_{\text{Acceleration of water observed from vessel of zero velocity}} = \underbrace{\frac{d|\mathbf{R}|}{dt} \mathbf{T}_R + |\mathbf{R}| \frac{d\mathbf{T}_R}{dt}}_{\text{Acceleration of water observed from vessel of velocity } \mathbf{P}} \quad (31)$$

when unit tangents $\mathbf{T}_D = \mathbf{D}/|\mathbf{D}|$ and $\mathbf{T}_R = \mathbf{R}/|\mathbf{R}|$ exist, noting $d|\mathbf{D}|/dt = 0$.

Despite $d\mathbf{D}/dt$ and $d\mathbf{R}/dt$ being equal, equation (31) shows that their tangential components are generally unequal, as therefore are their normal components. While *doppelgängers* of sorts, $d\mathbf{D}/dt$ and $d\mathbf{R}/dt$ are thus not interchangeable. The tangential component of just one - that of $d\mathbf{R}/dt$ - can convey the spatial distribution of Gerstner's fluid particles and the normal component of just one - that of $d\mathbf{R}/dt$ - can convey the shape of Gerstner waves.

According to (31), a fluid particle that exhibits constant speed along a trajectory of constant curvature may simultaneously be seen to quicken and slow on a trajectory of sharp and gentle turns. In this way, Gerstner's particle reflects the Galilean principle: total acceleration is absolute, but it can be redistributed. Figure 6 illustrates how. Galilean transformations can rescale and / or redirect a body's tangential acceleration and normal acceleration.

Curiously, a particularly consequential Galilean transformation occurs at points where neither a particle's normal nor its tangential acceleration is resized or redirected. A case we encountered in (13), $d|\mathbf{R}|/dt = 0$ at trochoidal peaks and troughs (when $|\mathbf{R}| \neq 0$). Consulting (31), this case implies,

$$|\mathbf{D}| \left| \frac{d\mathbf{T}_D}{dt} \right| = |\mathbf{R}| \left| \frac{d\mathbf{T}_R}{dt} \right| \implies |\mathbf{D}|^2 \kappa_D = |\mathbf{R}|^2 \kappa_R \quad (32)$$

at the highest and lowest points in a fluid particle's path, whether it is observed to trace (circular) orbits of curvature κ_D or (trochoidal) wave profiles of curvature κ_R .

At a fluid particle's highest and lowest points then, equation (32) tells us that $|\mathbf{R}| > |\mathbf{D}|$ if and only if $\kappa_R < \kappa_D$ and that $|\mathbf{R}| < |\mathbf{D}|$ if and only if $\kappa_R > \kappa_D$. To a sailor who matches the wave velocity, particles appear faster at their lowest points than they do to the sailor at rest (see (6) and (8)).

That is, $|\mathbf{R}| > |\mathbf{D}|$ since $|\mathbf{R}| = |(1/G) + r||\omega|$ while $|\mathbf{D}| = r|\omega|$. As (32) predicts then, the troughs of gravity waves therefore curve less sharply than the circular orbits of fluid particles.

The picture at wave peaks is more nuanced. To a sailor who matches the wave velocity, fluid appears slower at its highest than it does to sailors at rest when $1/G < 2r$. In this case, $|\mathbf{R}| < |\mathbf{D}|$ since $|\mathbf{R}| = |(1/G) - r||\omega|$ while $|\mathbf{D}| = r|\omega|$. Equation (32) thus predicts that the peaks of gravity waves curve more sharply than the orbits of fluid particles when $rG > 1/2$.

Even when it preserves a particle's normal and tangential acceleration vectors, a Galilean transformation can thus reconfigure a body's acceleration. As (32) shows, the body's trajectory may sharpen at one extremum while broadening at the other. A trajectory that exhibits vertical extrema of equal curvature is transformed into one which does not (and vice versa).

What makes this so consequential is that such a transformation cannot take place in isolation. Equation (32) predicts that extrema of unequal curvature are formed by particles of unequal speed. To exhibit different speeds at peaks and troughs, some change in speed must take place in between. Hence, $d|\mathbf{R}|/dt \neq 0$ at some point(s) between the extrema. Since $d|\mathbf{D}|/dt = 0$ everywhere, particles thus exhibit a form of acceleration in a frame of velocity \mathbf{P} that they do not exhibit in a fixed frame. A Galilean transformation can therefore introduce or remove a body's capacity to draw closer to, or pull away from, another body on the same path.

The total acceleration of Gerstner's particles is thus reconfigured at a trajectory's extrema and redistributed away from extrema. Table 2 highlights two pronounced cases: one away from the extrema, one at an extremum.

Firstly, $d\mathbf{T}_R/dt = \mathbf{0}$ at any inflection of a trochoidal profile. At such instants, particles exhibit entirely normal acceleration in a frame of zero velocity, but entirely tangential acceleration in a frame of velocity \mathbf{P} (see (31)). Evidently, trajectories which undergo no change in concavity can be transformed into ones which do (and vice versa).

Secondly, $d\mathbf{T}_R/dt$ does not exist at cusps. Unit tangent \mathbf{T}_R does not exist at these cusps either. As such, the right hand side of (31) breaks down at

cusps, because \mathbf{T}_R and corresponding unit normal $\mathbf{N}_R = d\mathbf{T}_R/dt / |d\mathbf{T}_R/dt|$ cannot form a basis for acceleration, $d\mathbf{R}/dt$. Thus, a regular point in a body's trajectory can be transformed into a singularity (and vice versa) by moving between reference frames of uniform velocity.

It is important to note that the right hand side of (31) does not break down at all singular points. Although no trochoidal node exhibits a unique unit tangent (e.g. see Figure 9), either of a node's two unit tangents can, together with its respective normal, form a basis for acceleration, $d\mathbf{R}/dt$.

In summary, Galilean transformations are richer than their fundamental property might suggest. Whether a body of velocity \mathbf{v} is observed from a vessel of uniform velocity \mathbf{f} or from a vessel of uniform velocity \mathbf{g} , Galileo says that body appears to exhibit an acceleration equal to $d\mathbf{v}/dt$. That is,

$$\frac{d(\mathbf{v} - \mathbf{f})}{dt} = \frac{d(\mathbf{v} - \mathbf{g})}{dt} = \frac{d\mathbf{v}}{dt} \quad (33)$$

by Galilean relativity (because $d\mathbf{f}/dt = d\mathbf{g}/dt = \mathbf{0}$).

What (33) conceals is the interplay between the components of $d(\mathbf{v} - \mathbf{f})/dt = d\mathbf{F}/dt$ and $d(\mathbf{v} - \mathbf{g})/dt = d\mathbf{G}/dt$ which preserves (33). A change to any one of the four - the normal component of $d\mathbf{F}/dt$, the tangential component of $d\mathbf{F}/dt$, the normal component of $d\mathbf{G}/dt$, or the tangential component of $d\mathbf{G}/dt$ - must be compensated by a change to at least one of the other three. By applying (28) to $d\mathbf{F}/dt = d\mathbf{G}/dt$, it is clear that,

$$\left(\frac{d|\mathbf{F}|}{dt} \right)^2 - \left(\frac{d|\mathbf{G}|}{dt} \right)^2 = |\mathbf{G}|^4 \kappa_G^2 - |\mathbf{F}|^4 \kappa_F^2$$

governs this scheme of compensation.

References

- [1] Franz Joseph von Gerstner. *Theorie der wellen samt einer daraus abgeleiteten Theorie der Deichprofile*, pages 127–138. Haase, 1804.
- [2] David Henry. On Gerstner's water wave. *Journal of Nonlinear Mathematical Physics*, 15(Suppl 2):87–95, 2008.
- [3] William Froude. On the rolling of ships. *Transaction of the Institution of Naval Architects*, 2:180–229, 1861.

[4] William John Macquorn Rankine. VI. On the exact form of waves near the surface of deep water. *Philosophical transactions of the Royal society of London*, (153):127–138, 1863.

[5] Alan P Trujillo and Harold V Thurman. *Essentials of oceanography*, volume 733, page 239. Pearson Upper Saddle River, NJ, 2017.

[6] Adolphe Ganot. *Elementary Treatise on Physics Experimental and Applied for the Use of Colleges and Schools*, page 36. W. Wood and Company, 1883.

[7] Jasper Flick. Waves, 2018. URL <https://catlikecoding.com/unity/tutorials/flow/waves/>. Accessed: 2025-10-05.

[8] George B Thomas, Ross L Finney, Maurice D Weir, and Frank R Giordano. *Calculus*. Boston: Addison-Wesley, 2001.

[9] Emma C Phillips. Custom waves, 2016. URL <https://www.desmos.com/calculator/8ruwco9oml>. Accessed: 2025-10-05.

[10] Mark Danovich. Wave circles, 2016. URL <https://markd87.github.io/2016/05/06/wave-circles.html>. Accessed: 2025-10-05.

[11] David J Raymond. Chapter 1 Waves in two and three dimensions, 2020. URL <http://kestrel.nmt.edu/~raymond/classes/ph221/diff.pdf>. Accessed: 2025-10-05.

[12] Douglas M Considine and Glenn D Considine. *Van Nostrand's scientific encyclopedia*, page 3138. Springer Science & Business Media, 2013.

[13] George C King. *Physics of energy sources*, pages 306–308. John Wiley & Sons, 2017.

[14] Thai Marine Meteorological Center. Chapter 1 Water wave mechanics, 2002. Accessed: 2025-10-05.

[15] Morikazu Toda. *Nonlinear waves and solitons*, volume 5, page 15. Springer Science & Business Media, 1989.

[16] Alfred George Greenhill. The Rankine trochoidal wave. *Proceedings of the Royal Society of London. Series A, Containing Papers of a Mathematical and Physical Character*, 94(659):238–249, 1918.

[17] John L Lumley. Film notes for Eulerian and Lagrangian descriptions in fluid mechanics, 1969. URL <http://web.mit.edu/hml/ncfmf/01ELDFM.pdf>. Accessed: 2025-10-05.

[18] David Nelson. *The Penguin dictionary of mathematics*. Penguin UK, 2008.

[19] Carl Rod Nave. Ocean waves. URL <http://hyperphysics.phy-astr.gsu.edu/hbase/Waves/watwav2.html>. Accessed: 2025-10-05.

[20] Heidi Burgiel. Cusp on the cycloid, 2010. URL http://www.mit.edu/~h1b/1802/pdf/MIT18_02SC_notes_10.pdf. Accessed: 2025-10-05.

[21] Vipul Naik. Concavity, inflections, cusps, tangents, and asymptotes, 2011. URL <https://files.vipulnaik.com/math-152/concaveinflectioncusptangentasympotote.pdf>. Accessed: 2025-10-05.

[22] Hisashi Okamoto and Mayumi Shoji. *The mathematical theory of permanent progressive water-waves*, volume 20, page 85. World Scientific Publishing Company, 2001.

[23] Teepanis Chachiyo. Simple and accurate complete elliptic integrals for the full range of modulus. *arXiv preprint arXiv:2505.17159*, 2025.

[24] Lorenzo Sadun. Curvature and acceleration, 2015. URL <https://web.ma.utexas.edu/users/m408m/Display13-4-3.shtml>. Accessed: 2025-10-05.

[25] Sheila Widnall and Jaime Peraire. Lecture 16 - Intrinsic coordinates, 2009. URL https://ocw.mit.edu/courses/16-07-dynamics-fall-2009/84852a46fa77de9a750245ceb761255a/MIT16_07F09_Lec06.pdf. Accessed: 2025-10-05.

[26] Stanislaw R Massel. *Ocean waves breaking and marine aerosol fluxes*, volume 38, pages 11–12. Springer Science & Business Media, 2007.

[27] Alan Sokal. Handout #1: Newton's first law and the principle of relativity, 2017. URL https://www.ucl.ac.uk/~ucahad0/7302_handout_1.pdf. Accessed: 2025-10-05.